# Orbital-Selective Mott Phase in Multiorbital Models for Alkaline Iron Selenides $K_{1-x}Fe_{2-y}Se_2$

Rong Yu and Qimiao Si

*Department of Physics and Astronomy, Rice University, Houston, Texas 77005, USA*

(Received 11 September 2012; revised manuscript received 7 December 2012; published 3 April 2013)

We study a multiorbital model for the alkaline iron selenides $K_{1-x}Fe_{2-y}Se_2$ using a slave-spin method. With or without ordered vacancies, we identify a metal-to-Mott-insulator transition at the commensurate filling of six $3d$ electrons per iron ion. For Hund's couplings beyond a threshold value, this occurs via an intermediate orbital-selective Mott phase, in which the $3d$ $xy$ orbital is Mott localized while the other $3d$ orbitals remain itinerant. This phase is still stabilized over a range of carrier dopings. Our results lead to an overall phase diagram for the alkaline iron selenides, which provides a unified framework to understand the interplay between the strength of the vacancy order and carrier doping. In this phase diagram, the orbital-selective Mott phase provides a natural link between the superconducting $K_{1-x}Fe_{2-y}Se_2$ and its Mott-insulating parent compound.

DOI: 10.1103/PhysRevLett.110.146402 PACS numbers: 71.30.+h, 71.10.Hf, 71.27.+a, 74.70.Xa

*Introduction.*—It is generally believed that the superconductivity in iron-based materials [1,2] is unconventional and originates from electron-electron interactions. These materials, therefore, provide a new setting to address how strong electron correlations must be for the high-temperature superconductivity. For the parent iron pnictides, the metallic antiferromagnetic ground state [3] may arise either from the Fermi surface nesting of a weak coupling theory [4,5], or from the strong correlation effects associated with the proximity to a Mott transition and the concomitant quasilocal moments [6–12]. Here, indications for considerable electron correlations have come from a number of factors, including the large spectral weight in the fluctuating magnetic spectrum [13]. For the iron chalcogenides, the correlation effects are even more pronounced. In the 11 iron chalcogenides [14], both the large ordered magnetic moment and the ordering wave vector are difficult to understand within the nesting picture. In the iron oxychalcogenide $La_2O_3Fe_2Se_2$, the Mott insulating behavior has been experimentally identified and theoretically explained in terms of the band narrowing effect associated with the expansion of the iron lattice unit cell [15]. These results provide the support for the incipient Mott picture [16,17].

The recently discovered alkaline iron selenide superconductors [18] $A_{1-x}Fe_{2-y}Se_2$ ($A$ = K, Rb, Cs, or Tl) shed new light on this issue. In these materials the superconducting $T_c$ is comparable to that of the pnictides [18–21], and the superconductivity is near an insulating phase [22,23]. The insulator is antiferromagnetic with a large ordered moment [24,25]; importantly, this phase is intimately connected to the ordered iron vacancies [22,24,26]. The lack of hole pockets in the Fermi surface of the superconducting compounds revealed by the angle-resolved photoemission spectroscopy (ARPES) measurements [27–29] makes the high $T_c$ and the large-moment magnetic order hardly explainable by the nesting mechanism. Instead, they are more naturally understood within the incipient Mott picture. For instance, the insulating state is naturally interpreted as a Mott insulator (MI), not only because it would have been metallic—with or without the ordered vacancies—in the absence of interactions but also because the interactions are strong as inferred from the large ordered moment. It has been proposed that the vacancy order enhances the interaction effects by reducing the bandwidth [30–32]. At the same time, various experiments suggest that the superconducting state is either free of iron vacancies or vacancy disordered, and is intrinsically phase separated from the vacancy ordered insulating state [33–35]. In order to understand the implications of the behavior observed in the alkaline iron selenides for the overall physics of the iron-based superconductors, it is important to understand how the vacancy ordered insulating state connects to superconducting phase. Elucidating this linkage is an important goal of the present study.

In multiorbital systems, the physics of the metal-to-insulator transitions (MITs) [36] may be orbital sensitive. An extreme example is the orbital-selective Mott transition (OSMT), for which the Mott transition takes place at different correlation strengths for different orbitals [37,38]. It is believed that the OSMT occurs in $(Ca, Sr)_2RuO_4$ [37–39]. For iron-based superconductors, strong orbital differences have been suggested in several systems [40–43]. For the iron pnictides, an orbital-selective Mott phase (OSMP) is competitive but is not stabilized as a ground state [44].

In this Letter, we investigate the MIT in the $K_{1-x}Fe_{2-y}Se_2$ system using a slave-spin method [44,45]. We show that when the Hund's coupling is sufficiently strong, the Mott localization of the system is always via an OSMP, in which the $3d$ $xy$ orbital is Mott localized, while the other orbitals are still itinerant. This OSMP generally exists in both the iron vacancy ordered and disordered cases, and survives a range of carrier doping.

 © 2013 American Physical Society

It provides a necessary connection between the vacancy ordered insulating phase and the metallic normal state above $T_c$. Our results allow us to make contact with recent ARPES measurements in this system [46].

*Model and method.*—We consider a multiorbital Hubbard model for the $K_{1-x}Fe_{2-y}Se_2$ compound. The Hamiltonian reads $H = H_0 + H_{\rm int}$. Here, $H_0$ contains the tight-binding parameters among the five $3d$ orbitals, $H_0 = \frac{1}{2}\sum_{ij\alpha\beta\sigma} t_{ij}^{\alpha\beta} d_{i\alpha\sigma}^\dagger d_{j\beta\sigma} + \sum_{i\alpha\sigma}(\epsilon_\alpha - \mu) d_{i\alpha\sigma}^\dagger d_{i\alpha\sigma}$, where $d_{i\alpha\sigma}^\dagger$ creates an electron in orbital $\alpha = 1, \ldots, 5$ with spin $\sigma$ at site $i$, $\epsilon_\alpha$ is the on-site energy reflecting the crystal level splitting, and $\mu$ is the chemical potential. We have taken the tight-binding parameters from Ref. [47]. $H_{\rm int}$ contains on-site Coulomb interactions $H_{\rm int} = \frac{U}{2}\sum_{i,\alpha,\sigma} n_{i\alpha\sigma} n_{i\alpha\bar{\sigma}} + \sum_{i,\alpha<\beta,\sigma}[U' n_{i\alpha\sigma} n_{i\beta\bar{\sigma}} + (U' - J) n_{i\alpha\sigma} n_{i\beta\sigma} - J(d_{i\alpha\sigma}^\dagger d_{i\alpha\bar{\sigma}} d_{i\beta\bar{\sigma}}^\dagger d_{i\beta\sigma} - d_{i\alpha\sigma}^\dagger d_{i\alpha\bar{\sigma}}^\dagger d_{i\beta\bar{\sigma}} d_{i\beta\sigma})]$, where $n_{i\alpha\sigma} = d_{i\alpha\sigma}^\dagger d_{i\alpha\sigma}$. Here, $U$, $U'$, and $J$, respectively, denote the intraorbital repulsion, interorbital repulsion, and Hund's rule exchange coupling, which are assumed to be orbital independent and satisfy $U' = U - 2J$ [48].

The MIT of the above model is studied using a $U(1)$ slave-spin method [44]. Here, a slave $S = 1/2$ quantum spin is introduced to carry the charge degree of freedom, and the metallic (Mott insulating) state corresponds to the magnetically (dis)ordered state of the slave spins with the quasiparticle spectral weight in each orbital $Z_\alpha > 0$ ($Z_\alpha = 0$). This method allows proper treatment of Hund's coupling, and yields results that compare well with those from other methods such as the dynamical mean-field theory [45]. We perform the calculation at zero temperature [49], and drop the spin-flip and pair-hopping terms in $H_{\rm int}$ for simplicity. Including these terms leads to similar results [40]. We study the MIT on two two-dimensional lattices of iron ions: a regular square lattice sketched in Fig. 1(a) and a 1/5-depleted square lattice shown in Fig. 1(c). They respectively stand for the completely disordered and the perfect $\sqrt{5} \times \sqrt{5}$ iron vacancies.

*Metal-to-insulator transition.*—The results at the commensurate filling corresponding to $N = 6$ $3d$ electrons per Fe are summarized in the phase diagrams of Figs. 1(b) and 1(d). In both the vacancy disordered and ordered cases, the system experiences a Mott transition at $U_{\rm MT}$ from a metal to a MI with increasing $U$. The insulating phase is a low-spin MI for $J/U \lesssim 0.01$, but a $S = 2$ high-spin MI for larger $J$ values. $U_{\rm MT}$ first decreases then increases with an increasing $J/U$ ratio. Such a nonmonotonic behavior is a general feature of systems away from one electron per orbital, and is also obtained in the five-orbital model for the parent iron pnictides [44]. When the Hund's coupling is above a threshold ($J/U \gtrsim 0.1$), the system crosses over from a weakly correlated metal to a strongly correlated metal (SCM) with increasing $U$. The onset of this crossover (at $U^*$) is identified by a rapid drop of $Z_\alpha$ and a kink in the orbital filling in each orbital, as shown in Figs. 2(a)–2(d). In the SCM, $Z_\alpha$ is strongly orbital dependent. Increasing $U$ does not lead to the simultaneous Mott localization of all orbitals. The metallic state first crosses over to an intermediate OSMP at $U_{\rm OS}$. The Mott transition then takes place between the MI and the OSMP at a larger $U$.

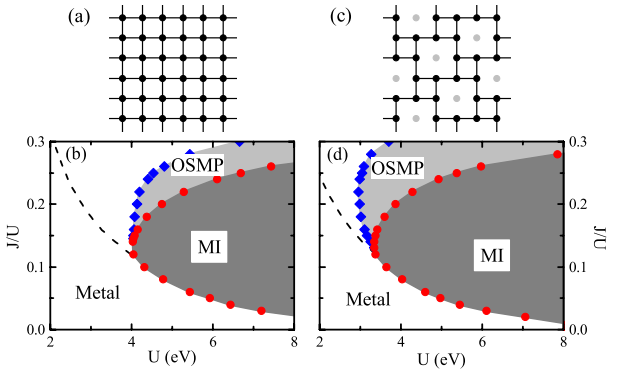


FIG. 1 (color online). (a), (c) The regular and 1/5-depleted square lattices, respectively, corresponding to the alkaline iron selenides with disordered and $\sqrt{5} \times \sqrt{5}$ ordered iron vacancies. (b), (d) Corresponding phase diagrams in the $J$-$U$ plane at filling $N = 6$ per Fe for the multiorbital model. The dark and light shaded regions respectively refer to the MI and the OSMP. The red circles and blue diamonds, respectively, denote the Mott transition and the crossover between the fully itinerant metal and OSMP. The black dashed line shows the crossover scale $U^*$ between the weakly and strongly correlated metals.

Importantly, the phase diagram of the vacancy ordered system is similar to that of its vacancy disordered counterpart. Quantitatively, $U_{\rm MT}$ and $U_{\rm OS}$ are, respectively, smaller in the vacancy ordered system, which reflects the ordered-vacancy-induced reduction in the kinetic energy and hence enhancement in the correlation effects [30].

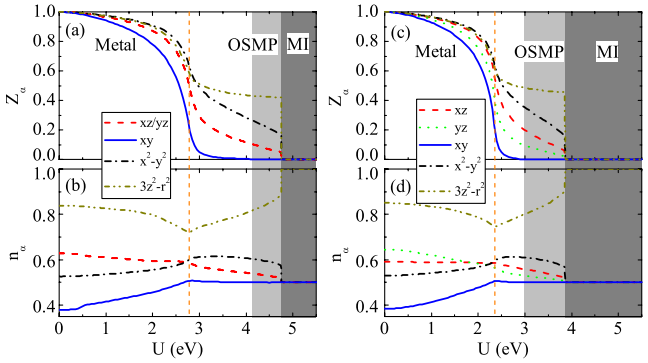


FIG. 2 (color online). (a), (b) Evolution of orbital resolved quasiparticle spectral weight $Z_\alpha$ [in (a)] and orbital filling factor (per iron site per spin) with $U$ for the multiorbital model at $N = 6$ and $J/U = 0.2$ on the regular lattice. The vertical dashed line indicates the position of $U^*$, which specifies the dashed line in Fig. 1(b). (c), (d) Same as (a) and (b) but on one of the two inequivalent sites of a unit cell of the 1/5-depleted lattice. $Z_\alpha$ for the $xz$ and $yz$ orbitals switch on the other site, as do the orbital filling factors.

*Nature of the orbital-selective Mott phase.*—As shown in Figs. 2(a) and 2(c), in the SCM regime, $Z$ in the $xy$ orbital is suppressed the most, and this orbital is very close to half-filling. Further increasing $U$ results in the Mott localization of the $xy$ orbital at $U_{\mathrm{OS}}$. The other orbitals remain itinerant up to $U_{\mathrm{MT}}$. The system is thus in an OSMP for $U_{\mathrm{OS}} < U < U_{\mathrm{MT}}$. We now turn to discussing the factors that stabilize the OSMP. For simplicity, we limit our discussion to the vacancy disordered case. The vacancy ordered case is qualitatively similar.

We start from the physics that governs the crossover between the weakly correlated metal and the SCM. Figure 3(a) plots the effective magnetic moment $S_{\mathrm{eff}} = \sqrt{\langle (S^z)^2 \rangle}$ as a function of $J/U$. It rapidly increases when the system passes through the crossover. Inside the SCM, $S_{\mathrm{eff}} \approx 2$, indicating that the $S = 2$ high-spin configuration, promoted by the Hund's coupling, is dominant in this regime.

The Hund's coupling also suppresses the interorbital correlations $C_{\alpha,\beta} = \langle n_\alpha n_\beta \rangle - \langle n_\alpha \rangle \langle n_\beta \rangle$, as shown in Fig. 3(a). Together with the crystal level splitting, this effectively decouples the $xy$ orbital from the others because in $K_{1-x}Fe_{2-y}Se_2$ the $xy$ orbital is the topmost level and is well separated from the others. For the same reason, this orbital is easier to be stabilized at half-filling for an overall filling of six electrons per Fe, as shown in Fig. 2(b) [and Fig. 2(d) for the vacancy ordered case]. Compared to the degenerate $xz/yz$ orbitals, which are also close to half-filling, the threshold value for the Mott localization in the nondegenerate $xy$ orbital is smaller.

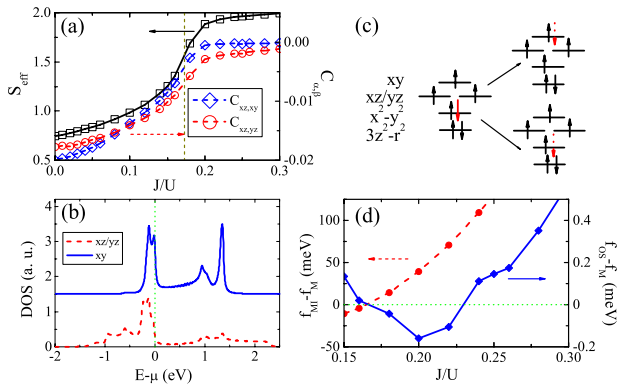


FIG. 3 (color online). (a) Evolution of the effective moment $S_{\mathrm{eff}}$ and interorbital correlations $C_{xz,xy}$ and $C_{xz,yz}$ with $J/U$ at $N = 6$ and $U = 3$ eV on the regular lattice. The vertical dashed line indicates the position of $U^*(J)$. (b) Orbital projected density of states in $xy$ and $xz/yz$ orbitals at the noninteracting limit ($J = U = 0$) of the same model. The curve for the $xy$ orbital is shifted upward for clarity. (c) Sketch of the two hopping processes of a charge excitation on the high-spin ground-state configuration that avoid the penalty from the repulsive interactions. (d) The differences in free energy density as a function of $J/U$ at $U = 4.2$ eV, showing the competition among the metallic (M), Mott insulating (MI), and orbital-selective (OS) Mott solutions.

Moreover, in the noninteracting limit the density of states (DOS) projected to the $xy$ orbital is narrower than those of other orbitals. For instance, as shown in Fig. 3(b), the ratio of the width of the DOS for the $xy$ orbital to that for the $xz/yz$ orbitals is about 0.6. (This is also the case for the vacancy ordered model; see the figure in the Supplemental Material [50]). This ratio is smaller than that for the LaOFeAs system, which is about 0.7. Hence, in $K_{1-x}Fe_{2-y}Se_2$, the $xy$ orbital contains less kinetic energy. Taking into account all the three factors, we find that in the SCM it is much easier to drive the $xy$ orbital toward the Mott localization. The result is the OSMP.

The threshold interaction for the OSMP, $U_{\mathrm{OS}}$, shows a strong dependence on $J$ especially when $J/U$ is large. This seems counterintuitive; one could expect that, if the $xy$ orbital is fully decoupled from the others, $U_{\mathrm{OS}}$ should approach the critical $U$ of a single-band Hubbard model, and hence should not depend on $J$. To understand the behavior of $U_{\mathrm{OS}}$, we examine the propagation of a charge excitation by assuming both $U$ and $J$ are large so that we may take the ground-state configuration to be the $S = 2$ high-spin state. A charge excitation with one more electron filled in the ground state can propagate via hopping to neighboring sites. $K_{xy}$ ($K_{\overline{xy}}$) denotes the kinetic energy gain associated with the hopping processes (not) involving the $xy$ orbital. Two representative hopping processes that do not disturb the high-spin ground-state configuration are illustrated in Fig. 3(c). Note that $K_{xy} < K_{\overline{xy}}$, not only because the $xy$ orbital has a narrower (noninteracting) bandwidth but also because the Hund's coupling suppresses the interorbital fluctuations. The Mott gap associated with either process is estimated as $\Delta_a = E(N+1) + E(N-1) - 2E(N) \approx U - 3J - K_a$, where $a = xy, \overline{xy}$. The difference in the kinetic energy gains leads to two different Mott gaps. $U_{\mathrm{OS}}$ ($U_{\mathrm{MT}}$) can be estimated as the $U$ value where the Mott gap $\Delta_a$ vanishes. Hence, we have $U_{\mathrm{OS}} \sim K_{xy}/(1 - 3J/U)$ and $U_{\mathrm{MT}} \sim K_{\overline{xy}}/(1 - 3J/U)$, both of which increase with $J/U$. This general consideration is consistent with our calculated phase boundaries for sufficiently large $J/U$. Interestingly, in this regime, increasing $J$ at a fixed $U$ leads to a delocalization from MI to OSMP, and then to the metallic phase. This is further confirmed by comparing the free energies of the three states, as shown in Fig. 3(d). Note that in the metallic phase, the interorbital correlations between the $xy$ orbital and others are substantially suppressed, but remain nonzero. The above argument on the behavior of $U_{\mathrm{OS}}$ does not hold for smaller $J/U$ where $U_{\mathrm{OS}}$ is close to $U^*$. In this regime, since the ground state mixes both high- and low-spin configurations, several mechanisms favoring either increasing or decreasing $U_{\mathrm{OS}}$ compete. As a result, $U_{\mathrm{OS}}$ shows complicated, even nonmonotonic, $J$ dependence [Fig. 1(b)].

*Orbital-selective Mott phase at finite dopings.*—Unlike the MI, which exists only at a commensurate filling, the OSMP can be stabilized at incommensurate fillings if

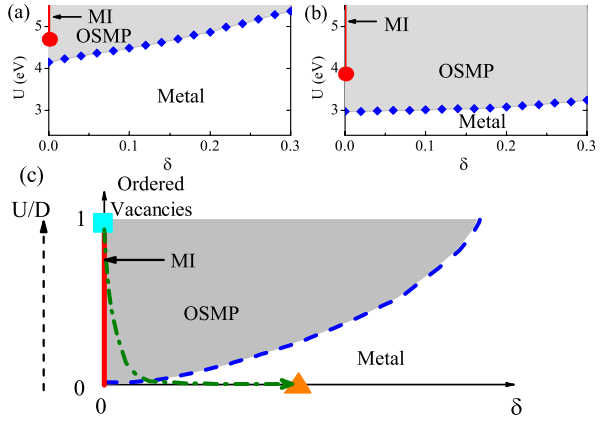


FIG. 4 (color online). (a), (b) Phase diagrams with $U$ and carrier doping concentration $\delta$ for the multiorbital model at $J/U = 0.2$ on the regular [in (a)] and the 1/5-depleted [in (b)] lattices, respectively. In either diagram, the large red dot refers to the Mott transition, and the blue diamonds show the orbital-selective Mott transition. (c) Sketch of a material-based phase diagram in the plane of carrier doping $\delta$ and ordered vacancies. The vacancy order parameter has been scaled to be between 0 and 1 (see text). The vacancy ordered insulating state is located as the cyan square in this phase diagram. The superconducting state is tentatively placed as the orange triangle on the $\delta$ axis. The dash-dotted line shows a possible route to connect the two phases. For realistic parameters, the Mott transition point is close to the origin, but could be either above or below it.

the chemical potential of the itinerant carriers falls inside the Mott gap of the localized orbital. In Figs. 4(a) and 4(b) we show the $U$ vs the carrier doping concentration ($\delta = N - 6$) phase diagrams for both the vacancy disordered and ordered cases. In both systems, the Mott transition takes place between a MI and an OSMP at the commensurate filling $\delta = 0$, and an OSMT between the OSMP and the metal extends to nonzero doping concentrations. In the vacancy ordered case, both the Mott transition and the OSMT take place at lower $U$ values compared to the vacancy disordered case, reflecting the enhanced correlations due to ordered vacancies.

*Unified phase diagram for alkaline iron selenides.*—The above results lead to a unified phase diagram, as sketched in Fig. 4(c). Here, the horizontal axis refers to the carrier doping $\delta$, and the vertical axis stands for the strength of the vacancy order. In general, a $K_{1-x}Fe_{2-y}Se_2$ system contains both vacancy ordered and disordered regimes. We may parametrize the strength of the vacancy order from 0 to 1 according to the volume fraction of the vacancy ordered regime (or, alternatively, to the potential strength of a virtual Fe atom, with the vacancy corresponding to an infinite potential). The two limiting cases along the vertical axis in the phase diagram, 0 and 1, are obtained from Figs. 4(a) and 4(b) at a fixed $U$ (which takes the value in real materials), respectively. The remaining part of the phase diagram can then be constructed by interpolating between the results in Figs. 4(a) and 4(b) at the same $U$. The resulting diagram consists of a MI, an OSMP, and a metal. The profile is similar to what are shown in Figs. 4(a) and 4(b) because, effectively, the ordered vacancies enhance the correlation $U/D$. (Here $D$ is a characteristic bandwidth of the multiorbital system.) The insulating compound with the $\sqrt{5} \times \sqrt{5}$ vacancy order is located at $\delta = 0$ and vacancy order 1 [cyan square in Fig. 4(c)]. On the other hand, we tentatively place the superconducting phase of the superconducting compounds at ambient pressure to be on the $\delta$ axis in the metallic state close to the OSMT [orange triangle in Fig. 4(c)]. We see that one physical trajectory going from the insulating phase to the superconducting one is for the dopants to both introduce extra carriers and suppress the vacancy order: the OSMP is an unavoidable intermediate phase connecting the two states.

The OSMP has direct experimental signature. In this phase, the quasiparticle spectral weight of the $xy$ orbital vanishes. Our prediction has recently been confirmed by ARPES measurements [46], which, in $K_{1-x}Fe_{2-y}Se_2$, have observed a rapid crossover into an OSMP. By measuring superconducting, insulating, and semiconducting $K_{1-x}Fe_{2-y}Se_2$, the ARPES study [46] has also provided evidence for the overall phase diagram we have derived for the alkaline iron selenides, with the superconducting phase being close to the OSMT.

It is instructive to put our results in broader contexts. Our results here connect to the general considerations about the orbital-dependent behavior [51] for the iron pnictides. In addition, while the OSMP appears here in the multiorbital Hubbard model, which is more pertinent to the iron-based materials than the Anderson-lattice model discussed in the context of high pressure effects on the iron pnictides [52], our results do relate to the studies of the orbital-dependent localization for quantum phase transitions in the latter model for correlated metallic systems. More generally, the OSMP reported here highlights in a particularly striking way the orbital sensitivity of the electron correlation effects, which is also important in a variety of transition-metal oxides [53].

In summary, we have studied the metal-to-insulator transition in the five-orbital Hubbard model for $K_{1-x}Fe_{2-y}Se_2$ with and without ordered vacancies. We find that the Mott localization of the system is via an intermediate orbital-selective Mott phase, in which the $3d$ $xy$ orbital is localized while the other $3d$ orbitals are itinerant. This phase persists over a range of carrier dopings. Finally, we have proposed a unified phase diagram for the alkaline iron selenides, with the orbital-selective Mott phase serving as the link between the insulating and superconducting compounds. Our results provide evidence that electron correlations play a vital role in the superconductivity of the iron-based superconductors.

We thank Z. K. Liu, D. H. Lu, Z. X. Shen, L. L. Sun, and M. Yi for useful discussions. This work has been supported

by the NSF and the Robert A. Welch Foundation Grant No. C-1411. Q. S. acknowledges the hospitality of the Aspen Center for Physics (NSF Grant No. 1066293) and the Institute of Physics of the Chinese Academy of Sciences.

*Note added.*—This work was reported in Ref. [54]. Complementary theoretical results on different systems using different methods have subsequently been reported in Refs. [55,56].


[1] Y. Kamihara, T. Watanabe, M. Hirano, and H. Hosono, J. Am. Chem. Soc. **130**, 3296 (2008).
[2] Z. A. Ren *et al.*, Chin. Phys. Lett. **25**, 2215 (2008).
[3] C. de la Cruz *et al.*, Nature (London) **453**, 899 (2008).
[4] J. Dong *et al.*, Europhys. Lett. **83**, 27006 (2008).
[5] S. Graser, T. A. Maier, P. J. Hirschfeld, and D. J. Scalapino, New J. Phys. **11**, 025016 (2009).
[6] Q. Si and E. Abrahams, Phys. Rev. Lett. **101**, 076401 (2008).
[7] T. Yildirim, Phys. Rev. Lett. **101**, 057010 (2008).
[8] F. Ma, Z.-Y. Lu, and T. Xiang, Phys. Rev. B **78**, 224517 (2008).
[9] C. Fang, H. Yao, W.-F. Tsai, J. P. Hu, and S. A. Kivelson, Phys. Rev. B **77**, 224509 (2008).
[10] C. Xu, M. Muller, and S. Sachdev, Phys. Rev. B **78**, 020501(R) (2008).
[11] J. Dai, Q. Si, J.-X. Zhu, and E. Abrahams, Proc. Natl. Acad. Sci. U.S.A. **106**, 4118 (2009).
[12] G. S. Uhrig, M. Holt, J. Oitmaa, O. P. Sushkov, and R. R. P. Singh, Phys. Rev. B **79**, 092416 (2009).
[13] M. Liu *et al.*, Nat. Phys. **8**, 376 (2012).
[14] W. Bao *et al.*, Phys. Rev. Lett. **102**, 247001 (2009).
[15] J.-X. Zhu, R. Yu, H. Wang, L. L. Zhao, M. D. Jones, J. Dai, E. Abrahams, E. Morosan, M. Fang, and Q. Si, Phys. Rev. Lett. **104**, 216405 (2010).
[16] Q. Si, E. Abrahams, J. Dai, and J.-X. Zhu, New J. Phys. **11**, 045001 (2009); Q. Si, Nat. Phys. **5**, 629 (2009).
[17] K. Haule and G. Kotliar, New J. Phys. **11**, 025021 (2009).
[18] J. Guo, S. Jin, G. Wang, S. Wang, K. Zhu, T. Zhou, M. He, and X. Chen, Phys. Rev. B **82**, 180520(R) (2010).
[19] L. L. Sun *et al.*, Nature (London) **483**, 67 (2012).
[20] A. Krzton-Maziopa, Z. Shermadini, E. Pomjakushina, V. Pomjakushin, M. Bendele, A. Amato, R. Khasanov, H. Luetkens, and K. Conder, J. Phys. Condens. Matter **23**, 052203 (2011).
[21] Y. Mizuguchi, H. Takeya, Y. Kawasaki, T. Ozaki, S. Tsuda, T. Yamaguchi, and Y. Takano, Appl. Phys. Lett. **98**, 042511 (2011).
[22] M. Fang, H.-D. Wang, C.-H. Dong, Z.-J. Li, C.-M. Feng, J. Chen, and H. Q. Yuan, Europhys. Lett. **94**, 27009 (2011).
[23] D. M. Wang, J. B. He, T.-L. Xia, and G. F. Chen, Phys. Rev. B **83**, 132502 (2011).
[24] W. Bao, Q.-Z. Huang, G.-F. Chen, D.-M. Wang, J.-B. He, and Y.-M. Qiu, Chin. Phys. Lett. **28**, 086104 (2011).
[25] M. Wang *et al.*, Nat. Commun. **2**, 580 (2011).
[26] F. Ye, S. Chi, W. Bao, X. F. Wang, J. J. Ying, X. H. Chen, H. D. Wang, C. H. Dong, and M. Fang, Phys. Rev. Lett. **107**, 137003 (2011).
[27] Y. Zhang *et al.*, Nat. Mater. **10**, 273 (2011).
[28] T. Qian *et al.*, Phys. Rev. Lett. **106**, 187001 (2011).
[29] D. Mou *et al.*, Phys. Rev. Lett. **106**, 107001 (2011).
[30] R. Yu, J.-X. Zhu, and Q. Si, Phys. Rev. Lett. **106**, 186401 (2011).
[31] Y. Zhou, D.-H. Xu, F.-C. Zhang, and W.-Q. Chen, Europhys. Lett. **95**, 17003 (2011).
[32] C. Cao and J. Dai, Phys. Rev. B **83**, 193104 (2011).
[33] Z. Wang, Y. J. Song, H. L. Shi, Z. W. Wang, Z. Chen, H. F. Tian, G. F. Chen, J. G. Guo, H. X. Yang, and J. Q. Li, Phys. Rev. B **83**, 140505 (2011).
[34] W. Li *et al.*, Nat. Phys. **8**, 126 (2012).
[35] F. Chen *et al.*, Phys. Rev. X **1**, 021020 (2011).
[36] M. Imada, A. Fujimori, and Y. Tokura, Rev. Mod. Phys. **70**, 1039 (1998).
[37] V. Anisimov, I. A. Nekrasov, D. E. Kondakov, T. M. Rice, and M. Sigrist, Eur. Phys. J. B **25**, 191 (2002).
[38] L. de'Medici, S. R. Hassan, M. Capone, and X. Dai, Phys. Rev. Lett. **102**, 126401 (2009).
[39] M. Neupane, P. Richard, Z.-H. Pan, Y.-M. Xu, R. Jin, D. Mandrus, X. Dai, Z. Fang, Z. Wang, and H. Ding, Phys. Rev. Lett. **103**, 097001 (2009).
[40] R. Yu and Q. Si, Phys. Rev. B **84**, 235115 (2011).
[41] Z. P. Yin, K. Haule, and G. Kotliar, Nat. Mater. **10**, 932 (2011).
[42] L. Craco, M. S. Laad, and S. Leoni, Phys. Rev. B **84**, 224520 (2011).
[43] T. Yoshida *et al.*, arXiv:1205.6911.
[44] R. Yu and Q. Si, Phys. Rev. B **86**, 085104 (2012).
[45] L. de'Medici, A. Georges, and S. Biermann, Phys. Rev. B **72**, 205124 (2005).
[46] M. Yi *et al.*, Phys. Rev. Lett. **110**, 067003 (2013).
[47] R. Yu *et al.*, arXiv:1103.3259.
[48] As is typical, $U$, $U'$, and $J$ are only weakly orbital dependent, and satisfy $U' = U - 2J$ based on symmetry considerations; see C. Castellani, C. R. Natoli, and J. Ranninger, Phys. Rev. B **18**, 4945 (1978). In this paper, we thus take them as orbital independent. One of our important conclusions is that an orbital-selective Mott phase arises even in this case.
[49] We focus on the behavior in the normal state, and will therefore not consider the pairing instability which is expected to yield a superconducting phase in the metallic phase close to the Mott transition.
[50] See Supplemental Material at http://link.aps.org/supplemental/10.1103/PhysRevLett.110.146402 for detailed information on the density of states in the vacancy ordered model.
[51] R. R. P. Singh, arXiv:0903.4408.
[52] A. Hackl and M. Vojta, New J. Phys. **11**, 055064 (2009).
[53] T. Hotta, Rep. Prog. Phys. **69**, 2061 (2006).
[54] R. Yu and Q. Si, http://meetings.aps.org/link/BAPS.2012.MAR.Z22.13.
[55] Z. P. Yin, K. Haule, and G. Kotliar, Phys. Rev. B **86**, 195141 (2012); **86**, 239904(E) (2012).
[56] E. Bascones, B. Valenzuela, and M. J. Calderon, Phys. Rev. B **86**, 174508 (2012).